

# Electron Spectroscopy for Material Characterization

Şefik SÜZER

*Bilkent University, Chemistry Department,  
06533 Ankara-TURKEY*

Received 04.05.1998

Basic principles of the two electron spectroscopic techniques, the x-ray photoelectron spectroscopy, XPS, and the Auger electron spectroscopy, AES, are given. Their utilization in material characterization are introduced through examples with application of these techniques to various surface related problems.

## Introduction

The techniques utilizing the detection of emitted electrons as a result of exposure to energetic photons (X-ray Photoelectron Spectroscopy, XPS) or electrons (Auger Electron Spectroscopy, AES) have emerged as versatile tools for material characterization especially in surface related areas<sup>1-5</sup>. In both XPS and AES all atoms except for H and He can be analyzed and the information derived stems from the atoms in the top 1-10 nm layers of the materials under investigation. The analysis depth can also be extended to about  $10^3$ - $10^4$  nm, however, only by incorporation of additional etching techniques. Sputtering or ion-milling with energetic (1-5 keV) noble gas ions (like Ar<sup>+</sup>) are the most popular methods for depth-profiling<sup>6</sup>. After their introduction in late 1960s by Kai Siegbahn in Uppsala, both XPS and AES have revolutionized concepts in many fields of chemistry, physics and material sciences. Unfortunately, only in 1994 the first instrument, capable of doing both XPS and X-ray induced AES analyses, was set-up in Turkey in our laboratory. In this article, we give examples of utilization of this technique for different kinds of surface-related problems carried out in our laboratory.

## Basic Theory and Experimental Requirements

In XPS the sample is subjected to energetic photons (x-rays, with energy  $h\nu$  and the energy of the primary electrons (K.E.) produced as a result of photoemission process are analyzed. The sought-out information, the binding energy (B.E.) is obtained through the energy conservation equation:  $h\nu$  (known) = K.E. (measured) + B.E. The electrons appear as peaks having certain quantized energies and are designated according to the levels they are ejected from and they are designated as such i.e. F1s, Ca2p or Pb4f etc. The peaks for levels other than s are further split due to the spin-orbit coupling into doublets ( $p_{3/2}$ - $p_{1/2}$  or  $d_{5/2}$ - $d_{3/2}$  etc.). Three parameters give important information;

- (i) the value of the B.E. ,
- (ii) the intensity at that particular energy  $I(\text{B.E.})$ ,

(iii) the angular dependency of the intensity  $I(\Theta)$ .

In AES the energy (K.E.) of the secondary electrons which are formed during the filling up of the initial core holes created by either the photoionization and/or electron-impact ionization are analyzed. The energy of these so-called Auger electrons are independent of the way in which the initial core-holes are created and are characteristic of the atoms present in the sample. The Auger electrons are designated by three letters indicative of (i) the level of the initial hole, (ii) the level from which the electron drops to fill the hole, and (iii) the level which the electron is ejected from. Hence  $\text{Na}_{KLL}$  refers to the process where the initial K hole (1s level) is filled by an electron from the L (2s or 2p) level and another L electron is ejected. The energy levels of a typical atom (magnesium) and the XPS, AES and the related process through which x-rays are created, XRF, are depicted in Figure 1. Accordingly, in the XPS spectrum of Mg in addition to the valence band (0-10 eV), a Mg2p spin-orbit doublet at around 50, a Mg2s peak at 90 and a Mg1s peak at around 1300 eV binding energies should be detected. Auger peaks having kinetic energies around 1100-1200 eV corresponding to KLL transitions should also be observed. In the XRF process, however, an energetic photon not an electron is produced.

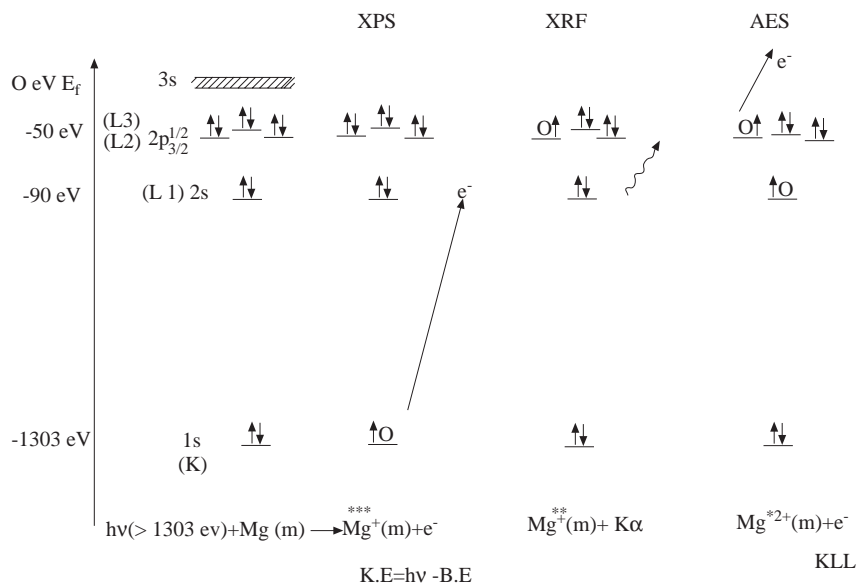


**Figure 1.** A schematic of the energy levels of Mg, the XPS, AES and XRF processes

Since it is the electrons which are analyzed and to avoid scattering of them by the residual gas molecules and also to enhance the surface sensitivity both techniques are performed under ultra-high-vacuum (UHV) conditions which require pressures better than  $10^{-9}$  torr. In principle any solid sample in the form of a film or a pressed powder can be analyzed without any chemical/physical pretreatment (unlike electron microscopic techniques).

The electrons are also severely scattered by the solid environment where they are created and only the ones created at or near the surface can survive without inelastic energy losses. This very property is what makes these techniques surface sensitive. The escape depth of the electrons which is defined as three times the attenuation length ( $\lambda$ ) of the electrons within a given material which depends on the material as well as the energy of the electrons but vary typically between 1-10 nm for electrons having energies between  $10^2$ - $10^3$  eV and for most inorganic and organic materials <sup>7</sup>.

Our instrument consists of a Kratos ES300 electron spectrometer with Al/Mg dual anode. The samples, in the form of films or pressed powders, are introduced directly from atmospheric pressure by a fast-lock entry compartment and the base pressure is kept below  $2 \times 10^{-9}$  torr during analysis by combination of diffusion and ion-pumps. A 1-3 keV  $\text{Ar}^+$  ion-gun is used for depth profiling or brief cleaning of the surface of the samples.

## Qualitative Information

Figure 2 shows a typical electron spectrum of a stainless steel sample as introduced into the spectrometer (bottom part) and after brief surface cleaning with argon ions (top part) using unmonochromatized  $\text{MgK}\alpha$  x-radiation ( $h\nu = 1253.6$  eV). Spectra consists of features in the form of peaks at various binding (in actuality it is the kinetic energy which is measured energies which can be identified and assigned as shown in Table 1. As is evident O and C are also present in ample quantities on the surface of the material but can be removed by  $\text{Ar}^+$  ion etching. Fe, Cr and Ni are the main constituents but other elements like Na, Ca and Si are also present in this particular stainless steel sample.

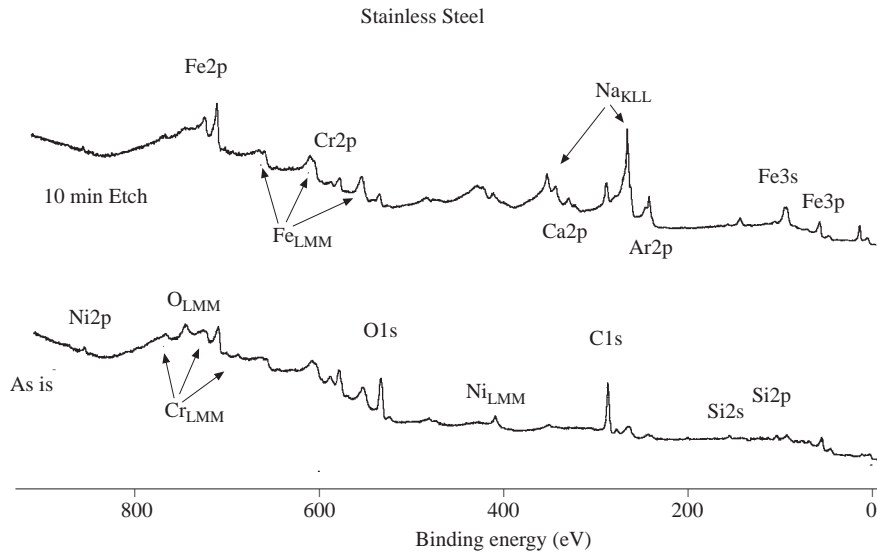


**Figure 2.** XPS and x-ray induced AES spectrum of a stainless steel sample before and after cleaning as a result of 10 min. 1 keV  $\text{Ar}^+$  etching.

## Quantitative Information

Relative quantification can be carried out using any photo and/or Auger peak corresponding to the particular element (with respect to another element present) using the appropriate cross-section of the peak and analyzer transmission function. For example the relative Fe to Cr atomic ratio can be calculated as follows:

$$Fe/Cr = \{I(Fe2p_{3/2})/I(Cr2p_{3/2})\} * \{\sigma(Cr2p_{3/2})/\sigma(Fe2p_{3/2})\} * \{K.E.(Fe2p_{3/2})/K.E.(Cr2p_{3/2})\}^n \quad (1)$$

where I refers to the peak intensity (area),  $\sigma$  refers to the photoionization cross-section<sup>8</sup>, K.E. is the kinetic energy of the peak and n is an instrumental factor which usually varies between 1 and 2. For our instrument

n is determined as 1.5. Using the parameters given in Table 1 and the experimentally determined peak areas the Fe/Cr atomic ratio can be determined as 2.8 and 3.2 before and after etching. Precision of the composition determination depends on the relative photoionization cross-section of the individual element but is in the range of 0.1-1%.

**Table 1.** XPS and Auger Peaks observed in Stainless Steel together with their Photoionization Cross-Sections towards MgK $\alpha$  x-rays (1253.6 eV).

Element	Level	B. E. (eV)	Cross Section <sup>a</sup> (Relative)	Auger Peak	K.E. (eV)
C	1s	285	1.00	KLL	263
O	1s	532	2.85	KLL	486
Na	1s	1072	7.99	KLL	994
Ar	2p	243	3.13		
	2s	320	1.71		
Ca	2p	348	5.13		
	2s	440	2.21		
Cr	3p	43	1.12	LMM	490
	3s	75	0.51	LMM	528
	2p <sub>3/2</sub>	574	7.60	LMM	570
	2s	696	3.23		
Fe	3p	53	1.58	LMM	599
	3s	92	0.63	LMM	648
	2p <sub>3/2</sub>	707	10.54	LMM	703
	2s	845	3.70		
Ni	3p	67	2.06	LMM	781
	3s	111	0.75	LMM	846
	2p <sub>3/2</sub>	853	13.92	LMM	863
	2s	1009	4.16		

<sup>a</sup> Reference 8.

## Chemical State Information

Often it is desirable to identify the chemical state (charge) of the element under investigation since many of the chemical/physical properties depend on this. This information is also inherent in the derived binding energy which shifts according to chemical and/or physical environment of the element. These so-called chemical shifts, although in principle calculable from first principles, involve many different kinds of parameters, hence, are best determined experimentally. Figure 3 displays part of the XPS spectrum of an electrochemically CdTe coated films for solar energy applications. On the surface of the films both Te 3d and 4d peaks have multiple spin-orbit doublets which can be assigned to telluride (2-) and oxytelluride ( $\delta+$ ) chemical states whereas both the Cd3d and 4d peaks are simple doublets assigned to cadmium (2+) chemical state. Relative intensities of an nd spin-orbit doublet corresponding to the 5/2 and 3/2 total angular momentum states are given by  $(2 \times 5/2 + 1) : (2 \times 3/2 + 1) = 6:4$  which are separated by the corresponding spin-orbit splitting energies which are 10.4, 6.7 and 1.8 eV for the Te3d, Cd3d and Te4d levels, respectively, and the corresponding splitting is smaller than our instrumental resolution of 1.5 eV for the Cd4d level. The

chemical shift between the 2- and the  $\delta+$  states of tellurium can be determined from the energy difference between the corresponding  $3d_{5/2}$  peaks as 3.4 eV where the binding energy of the oxytelluride is higher since the electron experiences a higher potential. After removal of the nonstoichiometric surface layers by etching the stoichiometric CdTe can be observed as shown on the upper region of the figure. Determination of the optimum conditions for obtaining a stoichiometric CdTe coating (as determined by XPS) was demonstrated to be very important for performance of these solar collectors prepared by electrochemical methods<sup>9</sup>.

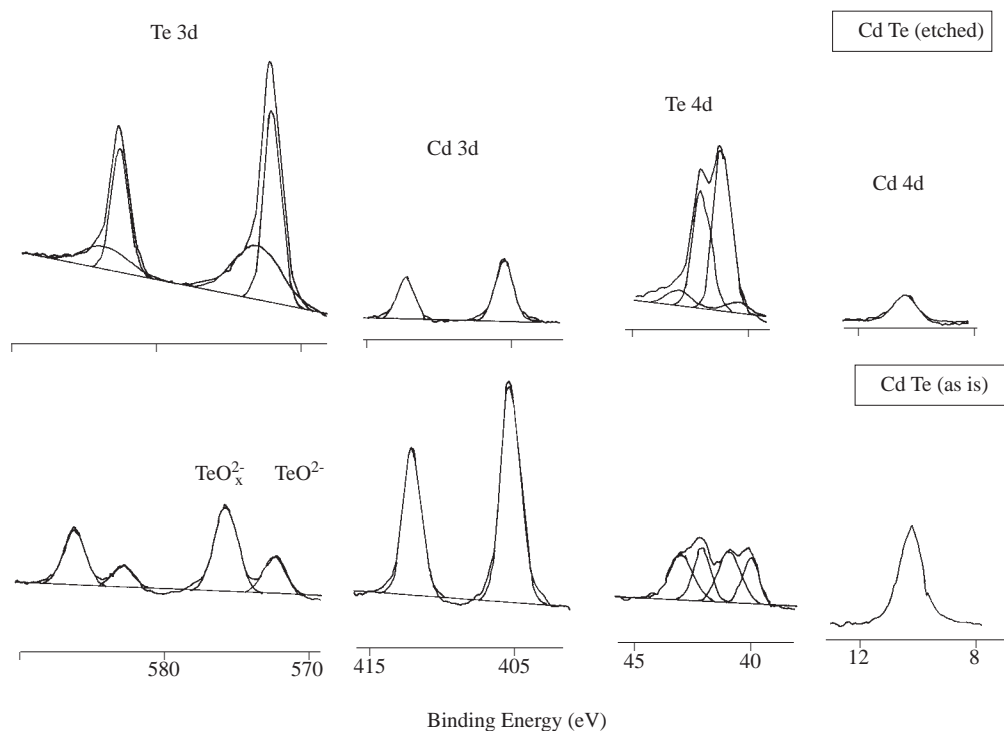


**Figure 3.** Relevant parts of XPS spectrum of electrodeposited CdTe on ITO substrate also before and after ion etching.

Chemical state changes can also be followed during a certain process as exemplified in Figure 4 where both Ru 3d and N1s levels are followed during thermal decomposition of a  $\text{Ru}(\text{NO})(\text{NO}_3)_3$  catalyst precursor. Before annealing the Ru is at 4+ state (as designated by A in Figure 4) and two different nitrogens ( $\text{NO}_3$  and NO) with the correct stoichiometric ratio of 3:1 are present. During annealing  $\text{NO}_3$  is lost initially with the corresponding shift of Ru to 3+ first (B) followed by 2+ (C) after losing all of nitrogens metallic Ru (D) is also observed. When the same precursor is analyzed on silica support thermal decomposition is prevented as a result of a host-guest interaction and only in the presence of  $\text{H}_2$  a similar decomposition/reduction could be realized<sup>10</sup>.

Chemical shifts in the C1s level for different types of carbon and substituents are very important in polymer characterization. Certain agents concentrate very effectively at the surface of materials which can be an asset for certain applications (and nuisance for others). Such as the case for silicon containing polymeric materials<sup>11</sup>. Due to the very low surface energy siloxane containing groups dominate the surfaces when blended or copolymerized with other polymers. In a similar study we investigated the surface composition of the hydroxy-terminated poly( $\epsilon$ -caprolactone, PCL) / poly(dimethylsiloxane, PDMS) triblock copolymers using XPS and were able to show that the PDMS microdomains were segregated in the surface region to minimize the surface energy<sup>12</sup>. The result of a similar investigation is shown in Figure 5 where part of

XPS spectra of methyl methacrylate (MMA) and triethoxyvinylsilane (TEVS) polymerized using  $60\text{Co}$  ( $\gamma$ -radiation) together with their copolymers and blends are displayed. The spectrum of the blend which contains 90% PMMA and 10 % PTEVS is completely dominated by features assigned to PTEVS since the latter is very surface active. Through copolymerization in which the TEVS composition can be as high as 70% in the feed a reasonably mixed PMMA/PTEVS random copolymers can be achieved as also depicted in the figure<sup>13</sup>.

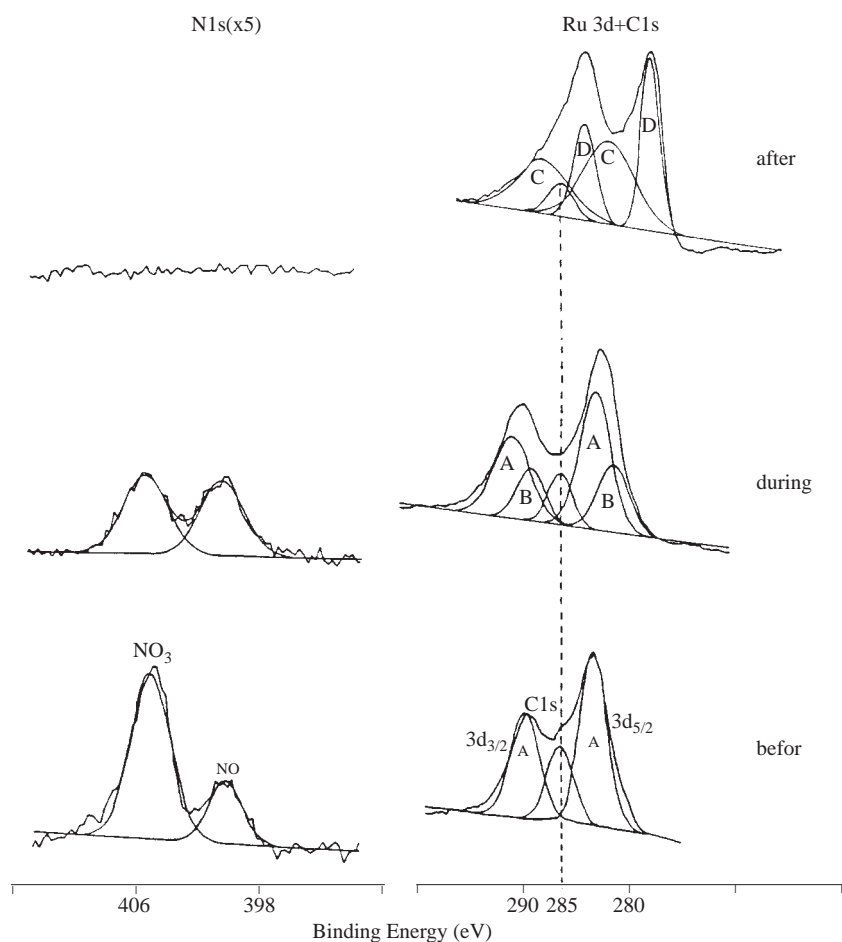


**Figure 4.** Ru3d and N1s regions of XPS spectrum of a  $\text{Ru}(\text{NO})(\text{NO}_3)_3$  catalyst precursor before, during and after annealing. As NO and subsequently  $\text{NO}_3$  are lost Ru is reduced from 4+ to metallic state successively.

Shifts due to physical environment can also be determined as shown in Figure 6 where the binding energy of the Au4f doublet at its metallic state are displayed when gold is deposited under different conditions<sup>14</sup>. Careful investigations also revealed chemical shifts due to particulate (cluster) size for gold colloids<sup>15</sup>.

The Auger peaks also display chemical shifts and in some cases the shifts can be larger than those on XPS peaks. Such a situation arises in the Al XPS 2p peak and the Auger KLL peak as shown in Figure 7. The chemical shift between the  $\text{Al}^{3+}$  (in  $\text{Al}_2\text{O}_3$ ) and  $\text{Al}^0$  (in metallic state) is 5.5 eV in the KLL peaks and only 2.7 eV in the Al2p peaks. Combination of the chemical shifts in the photo lines together with those on the Auger ones can lead to another experimentally derivable parameter, the Auger parameter<sup>16</sup> which can give even more precise chemical/physical state information as was demonstrated for Ni pigmented  $\text{Al}_2\text{O}_3$  solar collectors. Using the Al Auger parameter it was determined that the Ni pigmented sample was similar

to the anodized aluminum rather than  $\text{Al}_2\text{O}_3$  <sup>17</sup>.

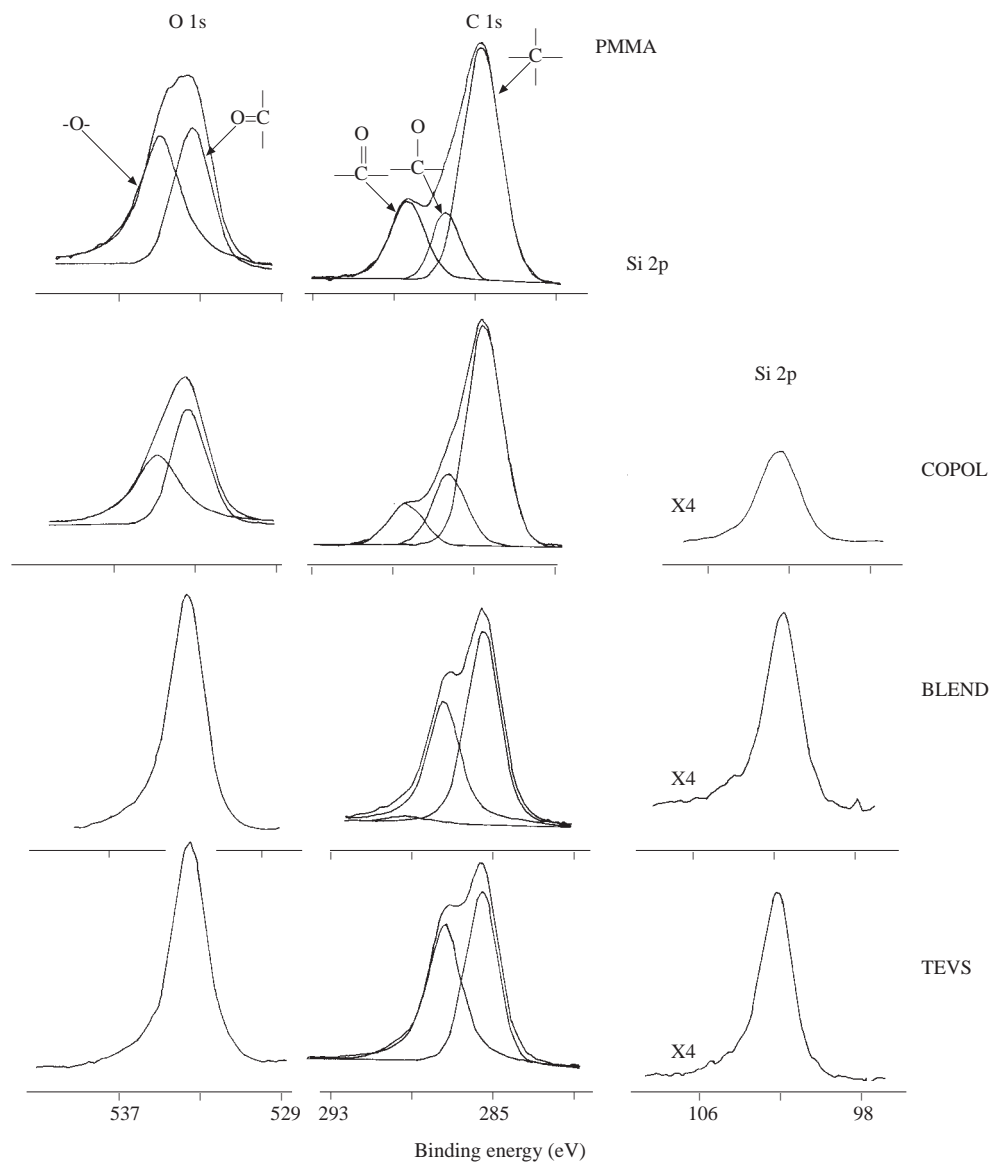


**Figure 5.** O1s, C1s and Si2p regions of  $^{60}\text{Co}$   $\gamma$ -ray induced PMMA and PTEVS together with their 10% PTEVS and 90 % PMMA blend. The spectrum of the blend is completely dominated by PTEVS. Whereas the spectrum of the corresponding copolymer where the initial feed contained 70 % TEVS and 30 % MMA displays features representing both of the polymers.

## Depth Information

### i-Angle Resolved XPS

The position of the electron energy analyzer with respect to the sample can be altered to vary the analysis depth of a given sample as shown in Figure 8. The result is a change in the electron take-off angle and hence

a longer escape depth for electrons stemming from the layers below the surface affecting the attenuation of the intensity of the electrons belonging to bulk atoms with respect to those on the surface.

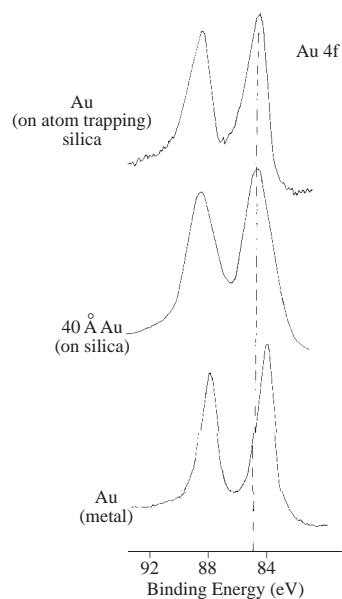


**Figure 6.** When gold is deposited on silica the binding energy of the 4f levels shift about 0.7 eV with respect to the metal although both are zerovalent. This information was used to assign the chemical state of gold deposited on an atom-trapping silica for use in signal enhancement in AAS<sup>14</sup>.

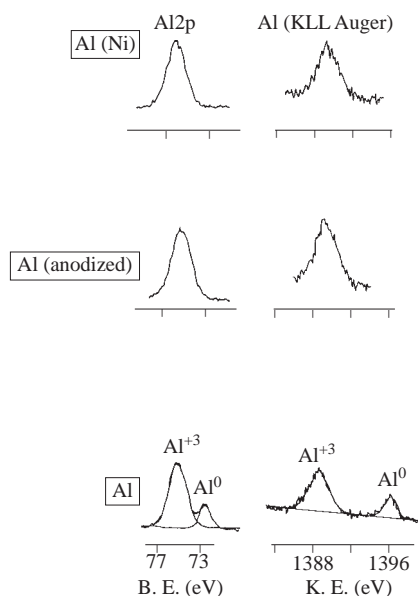


**Figure 7.** Al<sub>2</sub>p and Al KLL peaks of metallic and anodized aluminum samples. The metal has about 3 nm native oxide hence peaks belonging to both Al<sup>0</sup> and Al<sup>3+</sup> are observed. The chemical shift in the Auger peaks are more enhanced when compared with XPS peaks. The figure also displays the spectrum of Ni-pigmented aluminum solar collector where, using the Auger parameter obtained by combining the XPS and Auger shifts, it was demonstrated that the Al resembled anodized aluminum rather than Al<sub>2</sub>O<sub>3</sub><sup>17</sup>.

An analytical procedure has been developed to estimate the thickness by making use of such angle-dependency if the surface and bulk atoms have different chemical shifts such in the case of W4f levels of tungsten coated glasses. In Figure 8 the W4f levels at two different electron take-off angles ( $90^\circ$  and  $30^\circ$ ) are also given where the intensity of the metal peaks are clearly attenuated with respect to oxide ones. The thickness,  $d$ , of the oxide-overlayer can be calculated using the formula;

$$I_{WO_x}/I_W = \{1 - \exp(-d/\lambda \cdot \sin \theta)\} / \{\exp(-d/\lambda \cdot \sin \theta)\} \quad (2)$$

where  $\lambda$  is the attenuation length and  $\theta$  is the electron take-off angle with respect to the surface normal. Using the experimentally determined parameters one can obtain a thickness of approximately 4.5 nm for this native tungsten oxide<sup>6</sup>. This method is quick and versatile probe for deciding whether or not some element or a certain functional group is concentrated on the surface but is applicable only to uniform layers having thickness less than 10 nm.

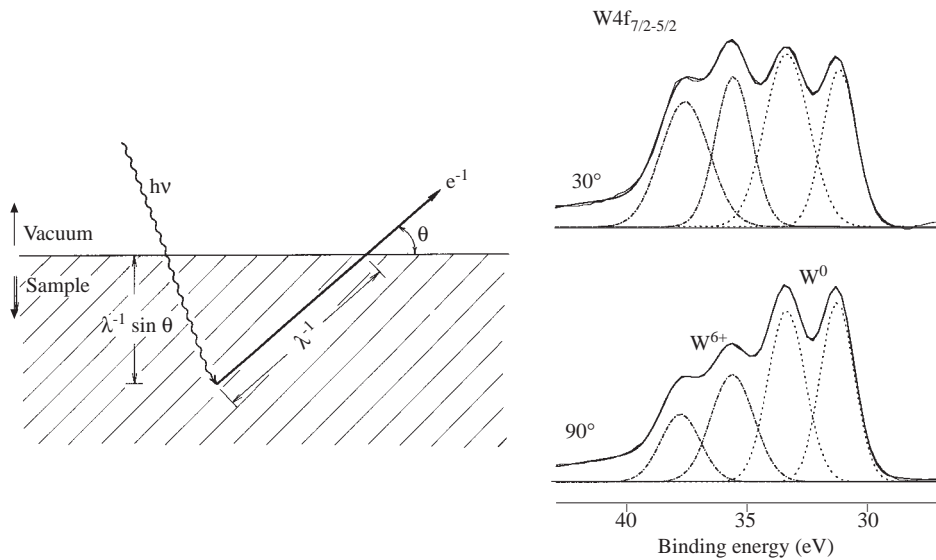


**Figure 8.** An schematic diagram of the electron take-off angle  $\theta$  is shown.  $\lambda$  is the electron's attenuation length. The XPS spectra of the 4f region of tungsten-coated glass recorded at  $90^\circ$  and  $30^\circ$  electron's take-off angles are also included. At the lower take-off angle the metallic peaks lose intensity with respect to oxide ones.

## ii- Chemical and/or $\text{Ar}^+$ Etching

This process utilizes the layer by layer removal either by chemical or physical means and subsequent analysis by XPS or AES. Both etching processes are known to be nonstoichiometric and can lead to serious errors in chemical state determination as well as quantification if precautions are not taken. They, nevertheless, are very popular to map out the compositional variations from the surface into the bulk of the material (depth profiling). In Figure 9 spectra of an approximately 100 nm  $\text{TiO}_2$  coated glass at different etching periods are shown. As the coating level is depleted features representative of typical float glass appear; mostly  $\text{SiO}_2$  but also Na, Mg and Ca as well as Sn which adheres to the surface of the float-glass since the molten glass is poured onto a hot liquid Sn-bath for obtaining smooth surfaces<sup>18</sup>.

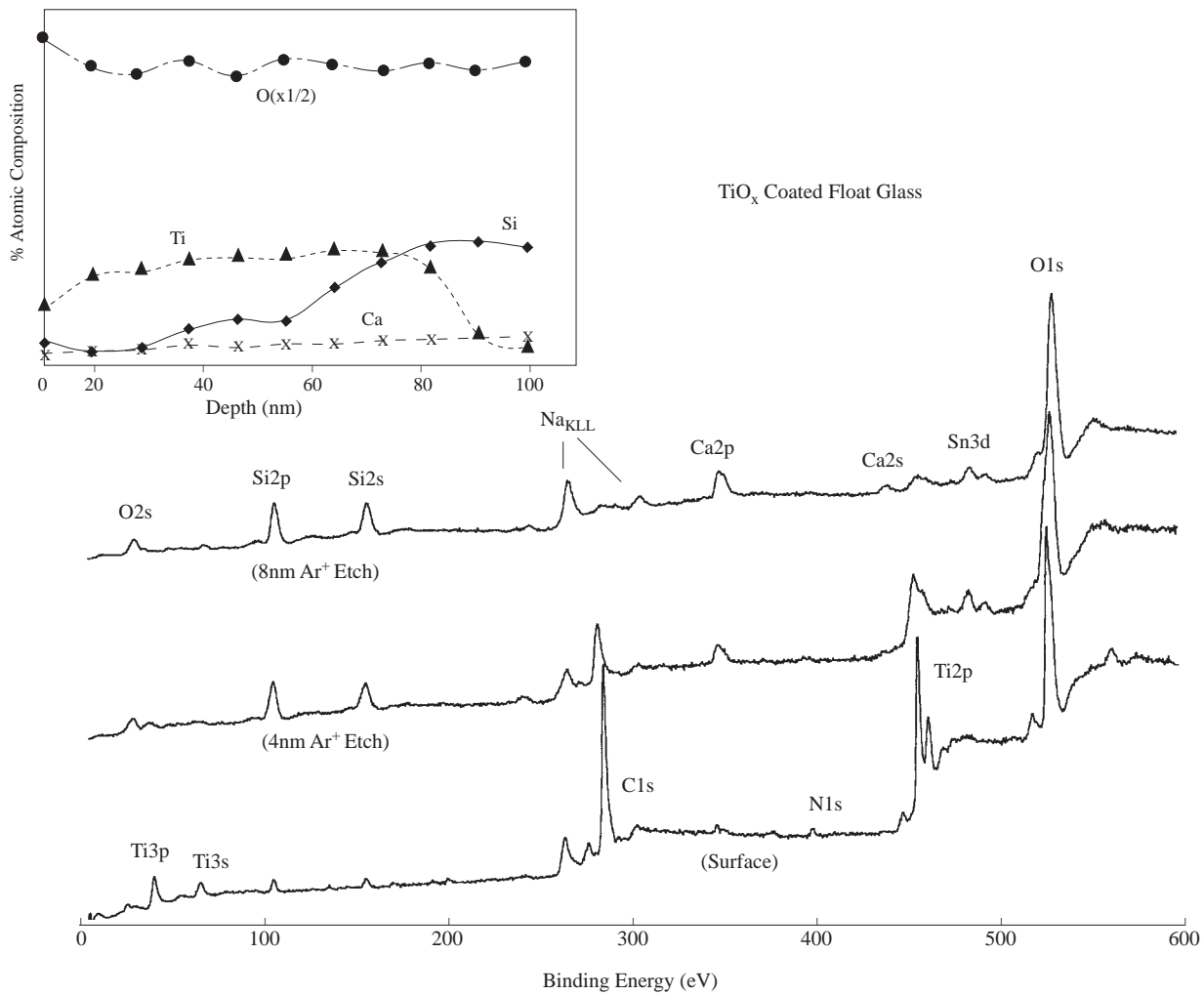


**Figure 9.** XPS spectra of about 80nm TiO<sub>2</sub> coated flont glass recorded at different etching periods (corresponding to different depths from the surface)

## Acknowledgments

I would like to express my sincere appreciation to my collaborators; Prof. Dr. G. C. Allen (Bristol, UK), O.Y. Ataman (METU), Prof. B.M. Baysal (Marmara Research Center), Dr. T. Çaykara (G. U.), Prof. H. Demiryont (Şişe-Cam), Prof. Dr. O. Güven (H. U.), Prof. Dr. F. Kadirgan (İTU), Mr. Ş. Sayan (Bilkent U.) and Prof. Dr. D.O. Uner (METU) for innumerable suggestions and contributions. Financial support of TÜBİTAK through grants TBAG-İ-15/7 and TBAG-COST-1 is kindly acknowledged.

## References

1. O. Nilsson, C.H. Norberg, J.E. Bergmark, A. Fahlman, C. Nordling and K. Siegbahn, **Helv. Phys. Acta** **41**, 1064-1095 (1968).

2. K. Siegbahn et.al. ESCA, Atomic, Molecular and Solid State Structure by Means of Electron Spectroscopy, Almqvist and Wiksells Boktryckeri AB, Uppsala (1967).
3. D.W. Turner, C. Baker, A.D. Baker and C.R. Brundle, Molecular Photoelectron Spectroscopy, Wiley-Interscience, London (1970).
4. J.H.D. Eland, Photoelectron Spectroscopy, Butterworths, London (1984).
5. G.K. Wertheim, **J. Electron Spectrosc.** **47**, 271-281 (1988).
6. D. Briggs and M. Seah, Practical Surface Analysis, Vol.1- Auger and X-Ray Photoelectron Spectroscopy, 2. Ed., Wiley, Chichester (1996).
7. C.J. Powell, **J. Electron Spectrosc.** **47**, 197-214 (1988).
8. J.H. Scofield, **J. Electron Spectrosc.** **8**, 129-137 (1976).
9. Ş. Süzer, Ş. Kutun and F. Kadirgan, **Fresenius J. Anal. Chem.** **355**, 384-86 (1996).
10. Ş. Sayan, Ş. Süzer and D.O. Uner, **J. Mol. Struct.** **410-411**, 111-14 (1997).
11. İ. Yılgör and J.E. McGrath, **Adv. Polm. Sci.** **86**, 1-85 (1988).
12. H.Y. Erbil, B. Yasar, Ş. Süzer and B.M. Baysal, **Langmuir** **13**, 5484-93 (1997).
13. T. Çaykara, O. Güven and Ş. Süzer, **Polymer** **39**, 5269-71 (1998).
14. Ş. Süzer, N. Ertaş, S. Kumser and O.Y. Ataman, **Appl. Spect.** **10**, 1537-39 (1997).
15. C. Battistoni, G. Mattogno and D.M.P. Mingos, **J. Electron Spectrosc.** **33**, 107-113 (1984).
16. C.D. Wagner and A. Joshi, **J. Electron Spectrosc.** **47**, 283-313 (1988).
17. Ş. Süzer, F. Kadirgan, H.M. Söhmen, A.J. Wetherilt and İ.E. Türe, **Sol. Energy Mater.** **52**, 55-60 (1998).
18. Ş. Süzer, T. Voscoboinikov, K.R. Hallam and G.C. Allen, **Fresenius J. Anal. Chem.** **355**, 654-656 (1996).